Neutron Star Tidal Deformabilities Constrained by Nuclear Theory and Experiment

Yeunhwan Lim[1,*] and Jeremy W. Holt[1,2,†]

[1]*Cyclotron Institute, Texas A&M University, College Station, Texas 77843, USA*
[2]*Department of Physics and Astronomy, Texas A&M University, College Station, Texas 77843, USA*

We confront observational data from gravitational wave event GW170817 with microscopic modeling of the cold neutron star equation of state. We develop and employ a Bayesian statistical framework that enables us to implement constraints on the equation of state from laboratory measurements of nuclei and state-of-the-art chiral effective field theory methods. The energy density functionals constructed from the posterior probability distributions are then used to compute consistently the neutron star equation of state from the outer crust to the inner core, assuming a composition consisting of protons, neutrons, electrons, and muons. In contrast to previous studies, we find that the 95% credibility range of predicted neutron star tidal deformabilities ($136 < \Lambda < 519$) for a 1.4 solar-mass neutron star is already consistent with the upper bound deduced from observations of the GW170817 event. However, we find that lower bounds on the neutron star tidal deformability will very strongly constrain microscopic models of the dense matter equation of state. We also demonstrate a strong correlation between the neutron star tidal deformability and the pressure of beta-equilibrated matter at twice saturation density.

Gravitational wave and electromagnetic signals from binary neutron star mergers offer a unique probe for studying the properties of ultradense matter. The recent observation of gravitational wave event GW170817 [1] and the associated electromagnetic counterpart [2] suggest the source to be a merger of two neutron stars with combined mass $M_{total} = 2.74^{+0.04}_{-0.01} \, M_\odot$ that left behind a relatively long-lived hypermassive neutron star remnant. Measurements of the late inspiral gravitational waveform from GW170817 were sufficient to place an upper limit of $\Lambda < 800$ on the tidal deformability [3,4] of a 1.4 $M_\odot$ neutron star, competitive with bounds [5] deduced from current neutron star mass and radius measurements. Subsequent works [6–12] have inferred constraints on a broader set of bulk neutron star properties such as the maximum mass [6–8,10,11], radii [6,7,12], and tidal deformabilities [9,12] from a combination of observational data and numerical relativity simulations. Ultimately, it will be equally important to infer complementary constraints on specific properties of the dense matter equation of state itself [13], such as the symmetry energy and its density dependence.

In the past, a wide range of models for the nuclear equation of state [14–19] have been used to investigate the neutron star tidal deformability. In the present Letter, our aim is to develop a framework that will enable statistical inferences of neutron star properties through the combination of laboratory measurements of nuclei and advances in microscopic modeling of the low- to moderate-density equation of state from chiral effective field theory (EFT) [20–22]. For this purpose, we construct parametric equations of state for symmetric nuclear matter and pure neutron matter, whose parameters

are sampled from a posterior Bayesian distribution function. The prior distribution functions are obtained from chiral effective field theory predictions for the nuclear equation of state up to twice nuclear saturation density, while the likelihood functions incorporate empirical information on the equation of state close to nuclear saturation density and for nearly isospin-symmetric matter. From this analysis, we demonstrate that an accurate description of the neutron star pressure at twice saturation density correlates strongly with the neutron star tidal deformability (see also Refs. [23,24]). This work builds upon previous studies [25–27] in which constraints from chiral effective field theory have been implemented in mean field modeling of the nuclear energy density functional.

Chiral effective field theory has been used in the past to predict neutron star radii and masses [28,29] and their impact on gravitational wave measurements [30] by extending the neutron matter equation of state to higher densities using piecewise polytropes. For instance, a 1.4 $M_\odot$ neutron star was found to have a radius in the range $9.5 < R < 13.5$ km. The stiffest equations of state considered in Ref. [28] generate neutron stars with a maximum mass up to nearly $M_{max} = 3 \, M_\odot$. Recent numerical relativity simulations [6–8, 10,11] that place an upper bound on the maximum mass of a nonrotating spherical neutron star, $M_{max} \lesssim 2.15$–$2.30 \, M_\odot$, may therefore help to rule out possible equations of state generated from extrapolating chiral effective field theory results to higher densities and thereby better constrain our theories of dense nuclear matter.

A main purpose of the present Letter is to investigate as well the extent to which lower bounds on the tidal

deformability [9] can reduce the range of allowed neutron star equations of state. In our modeling, the maximum neutron star mass falls below about $M < 2.3\ M_\odot$, but many of the equations of state produce $1.4\ M_\odot$ neutron stars with small tidal deformabilities. In particular, the suggested [9] lower bound on the binary tidal deformability $\tilde\Lambda > 400$ would rule out a large fraction of our equations of state and have important implications for lower bounds on neutron star radii.

We take as a starting point for the discussion a model of the bulk matter nuclear energy density functional of the form

$$\mathcal{E}(n,x) = \frac{1}{2m}\tau_n + \frac{1}{2m}\tau_p$$
$$+ (1-2x)^2 f_n(n) + [1-(1-2x)^2]f_s(n), \quad (1)$$

where n is the nucleon number density, τ_n and τ_p are the neutron and proton kinetic energy densities, x is the proton fraction, $f_s(n) = \sum_{i=0}^{3} a_i n^{(2+i/3)}$, and $f_n(n) = \sum_{i=0}^{3} b_i n^{(2+i/3)}$ has the same functional form with different expansion coefficients. We assume a quadratic dependence of the energy per particle on the isospin asymmetry, $\delta_{np} = (n_n - n_p)/(n_n + n_p)$, as in Refs. [31–34]. Variational calculations performed by Lagaris and Pandharipande [35] found that higher-order terms are negligible, even though a power series expansion in δ_{np} generically breaks down [36,37].

Joint probability distributions for the a_i and b_i coefficients can be obtained either from laboratory measurements of nuclei or from chiral effective field theory calculations of the nuclear equation of state. Given that chiral effective field theory provides a model-independent low-energy expansion of nuclear observables, where none of the parameters are fine tuned to the properties of bulk matter, we use the generated equations of state up to the density $n = 2n_0$, where $n_0 = 0.16$ fm^{-3}, to define prior distribution functions for the a_i and b_i. From the mean vectors and covariance matrices, we construct multivariate normal distributions for the (uncorrelated) a_i and b_i parameter sets. We then incorporate empirical information for the nuclear matter saturation density n_0, saturation energy B, incompressibility K, and skewness parameter Q into likelihood functions (see also Ref. [38]) from which we construct the final posterior distributions for the a_i. For the neutron matter equation of state, we include empirical constraints on the isospin-asymmetry energy J, its slope parameter L, curvature $K_{\rm sym}$, and skewness $Q_{\rm sym}$ to derive likelihood distributions involving the b_i. We neglect correlations between the symmetric nuclear matter and pure neutron matter bulk properties, since the uncertainties in J, L, $K_{\rm sym}$, and $Q_{\rm sym}$ are much larger than their counterparts in symmetric nuclear matter.

The chiral interactions considered in the present analysis have been used extensively in studies of nuclear dynamics

and thermodynamics (for recent reviews, see Refs. [39,40]). While the neutron matter equation of state is better constrained at low densities relative to the symmetric nuclear matter equation of state, at around twice nuclear saturation density the uncertainties are comparable [40–42]. Three-body forces are included at next-to-next-to-leading order (N2LO) in the chiral expansion, and progress toward the consistent inclusion of N3LO three-body forces is being made [43,44]. In order to estimate the theoretical uncertainties, we vary (i) the resolution scale $\Lambda_\chi \simeq 400$–500 MeV, (ii) the chiral order of the underlying nucleon-nucleon interaction [41,45–48] from N2LO to N3LO, and (iii) the order of the calculation in many-body perturbation theory. We have also reduced the fitting range from $\rho \le 0.32$ to $\rho \le 0.25$ fm^{-3} in order to check that our results are not especially sensitive to the choice of the transition density. In the inset to Fig. 1, we show the resulting nuclear (red) and neutron matter (blue) equation of state probability distributions up to $n = 2n_0$ from the prior probability distributions for a_i and b_i.

Gaussian likelihood functions incorporating empirical constraints on the quantities n_0, $B = -(E/A)|_{n_0}$, $K = 9n^2(\partial^2(E/A)/\partial n^2)|_{n_0}$, and $Q = 27n^3(\partial^3(E/A)/\partial n^3)|_{n_0}$ are obtained from Ref. [49] by analyzing 205 Skyrme force models. The marginal normal distributions for the nuclear matter properties have means and standard deviations: $n_0 = 0.160 \pm 0.003$ fm^{-3}, $B = 15.939 \pm 0.149$ MeV, $K = 232.65 \pm 7.00$ MeV, and $Q = -373.26 \pm 13.91$ MeV. In Fig. 1, the blue band is the resulting probability distribution for the nuclear matter equation of state up to $n = 1.0$ fm^{-3} obtained from the posterior probability distribution for the a_i.

For the equation of state of pure neutron matter, we construct the likelihood function involving the b_i starting
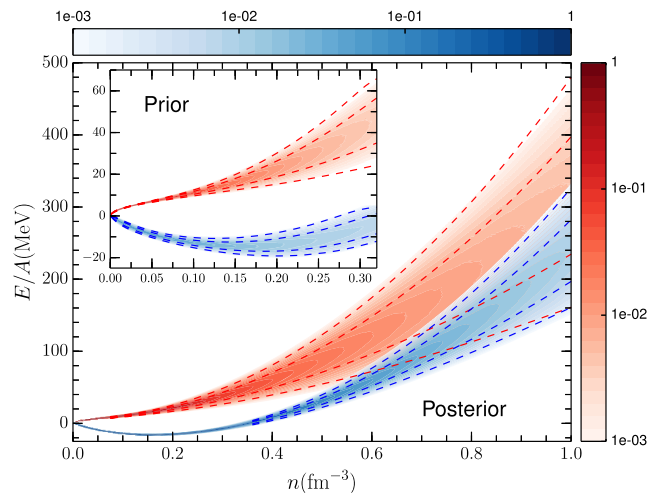

FIG. 1. Probability distributions for the symmetric nuclear matter (blue) and neutron matter (red) equations of state up to $n = 2n_0$ sampled from prior distributions derived from chiral EFT (inset). Equations of state up to $n = 1.0$ fm^{-3} sampled from posterior distributions for a_i and b_i in Eq. (1). The dashed lines denote the 1σ and 2σ probability contours.

from a conservative empirical constraint on the nuclear isospin-asymmetry energy $J = 31 \pm 1.5$ MeV [50]. To obtain constraints on the isospin-asymmetry slope parameter L, curvature K_{sym}, and skewness parameter Q_{sym}, we employ recent universal relations derived within a Fermi liquid theory description of nuclear matter [51]. This allows us to obtain the multivariate likelihood function associated with the b_i parameters. The red band in Fig. 1 shows the resulting neutron matter equation of state probability distribution function up to $n = 1.0$ fm^{-3} obtained by sampling over the posterior.

Once the energy density functionals in Eq. (1) are obtained, we construct the neutron star equation of state from the outer crust to the inner core. Certain combinations of the neutron matter and nuclear matter equations of state lead to unphysical behavior at very high densities. We ensure that the speed of sound remains subluminal for all densities present in the neutron star. In the end, we generate one million samples that we use for subsequent statistical analysis. Unlike many calculations of the tidal deformability Λ, we construct a realistic crust equation of state by employing the liquid drop model technique. This is a unified approach that allows the inclusion of nuclear pasta phases and is necessary for the consistent treatment of the neutron star equation of state. Additional details can be found in Ref. [25].

In Fig. 2, we show the mass vs radius distribution that results from our Bayesian statistical analysis. We have shown for comparison in the enclosed dashed region the mass vs radius constraints obtained by analyzing x-ray burst data from Steiner *et al.* [52]. We observe that, for a $1.4\,M_\odot$ neutron star, the radius lies within the range $10.36 < R < 12.87$ km and the distribution peaks at $R \simeq 12.10$ km. We find a relatively small probability for
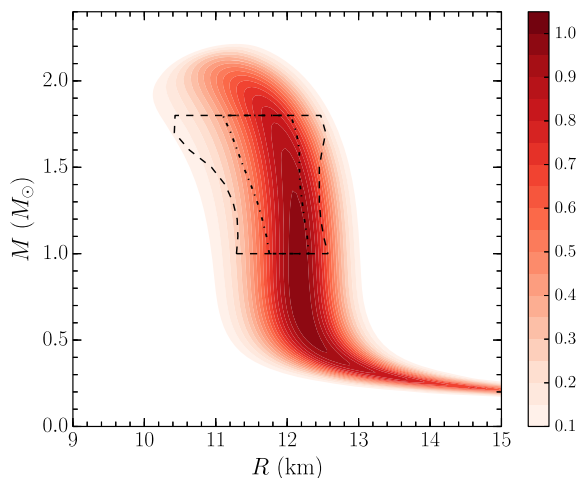
obtaining a maximum neutron star mass larger than $M_{max} = 2.2\,M_\odot$, but this may be the result of keeping only the four lowest powers of the Fermi momentum in the expansion of the energy density functional in Eq. (1) and the removal of equations of state with superluminal speeds of sound in our nonrelativistic framework. The recent numerical relativity simulations [6–8,10,11] that have predicted upper bounds on the neutron star maximum mass around $M_{max} \simeq 2.15$–$2.30\,M_\odot$ therefore do not impose additional constraints on our models.

In Fig. 3, we show the dimensionless tidal deformability and associated statistical uncertainties as a function of the neutron star mass. The red band denotes the 68% credibility interval, while the blue band denotes the 95% credibility interval. For a $1.4\,M_\odot$ neutron star, these bands correspond to the ranges $256 < \Lambda < 442$ and $136 < \Lambda < 519$, respectively. In contrast to previous work [12], the inferred upper bound on the tidal deformability $\Lambda < 800$ of a $1.4\,M_\odot$ neutron star from GW170817 does not strongly constrain our modeling. This may be due to the comparatively small value of the transition density $n = 1.1n_0$ chosen by Annala *et al.* at which the equation of state from chiral effective field theory is replaced by polytropic extrapolations. This choice was necessitated by the large theoretical uncertainties in Ref. [28] that arose from poorly constrained low-energy constants associated with the long-range two-pion-exchange three-body force. Recent analyses [53,54] have significantly reduced these uncertainties, enabling the construction of next-generation chiral nuclear forces [55,56] from which more reliable predictions for the equation of state beyond $n = n_0$ will be obtained. Our inclusion of chiral EFT predictions up to $n = 0.32$ fm^{-3} in constructing the prior distribution functions for b_i represents a maximal density limit at which chiral effective field theory calculations may be reliable, but when we reduced
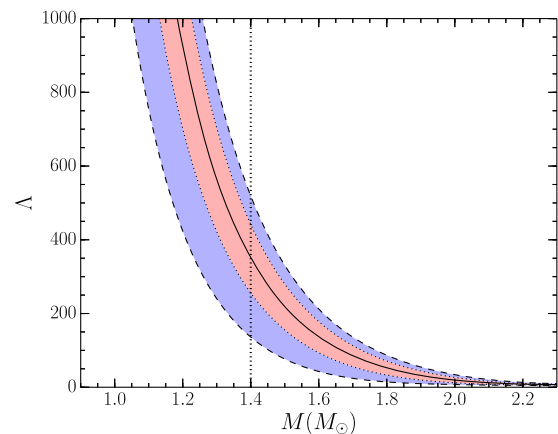

FIG. 2. Neutron star mass vs radius distribution obtained by sampling from the posterior distributions for a_i and b_i in Eq. (1). The central zone with dashed line represents the allowed area of mass and radius of neutron stars in Ref. [52].

FIG. 3. Dimensionless tidal deformability Λ as a function of neutron star mass M obtained from our posterior probability distributions. The red band is the 68% credibility interval and the blue band is the 95% credibility interval.
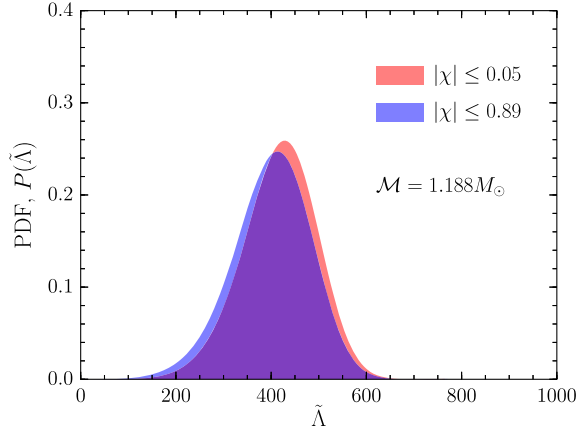
FIG. 4. Probability distribution function (PDF) for $\tilde{\Lambda}$ associated with the high-spin priors ($|\chi| < 0.89$) and low-spin priors ($|\chi| < 0.05$) mass distributions from the analysis of GW170817 in Ref. [1].

the fitting range to $n \leq 0.25$ fm^{-3}, we found no significant qualitative differences to our reported results.

Potentially much more restrictive to our present theories of the dense matter equation of state would be lower bounds on the tidal deformability, such as the recent suggestion [9] that $\tilde{\Lambda} > 400$ is needed for a binary neutron star merger remnant to avoid an immediate or short-timescale collapse to a black hole, where

$$\tilde{\Lambda} = \frac{16}{13} \frac{(m_1 + 12m_2)m_1^4\Lambda_1 + (m_2 + 12m_1)m_2^4\Lambda_2}{(m_1 + m_2)^5}. \quad (2)$$

In Fig. 4, we plot the probability distributions for $\tilde{\Lambda}$ assuming a chirp mass $\mathcal{M} = (m_1 m_2)^{3/5}/(m_1 + m_2)^{1/5} = 1.188\ M_\odot$ together with the high-spin priors ($|\chi| < 0.89$) and low-spin priors ($|\chi| < 0.05$) component mass distributions given in Ref. [1]. We observe that the binary tidal deformability distribution peaks at a value of $\tilde{\Lambda} = 402.23^{+147.72}_{-183.49}$ ($\tilde{\Lambda} = 418.11^{+142.02}_{-172.46}$) for high (low) spin, which extends well below the lower bound predicted in Ref. [9]. Note that the binary tidal deformability distribution in Fig. 4 comes from the statistical analysis of combined binary neutron star mass distributions [1] and our equation of state Λ distribution, not directly from gravitational wave analyses.

In the left panel of Fig. 5, we show the correlation between the tidal deformability Λ of a 1.4 $M_\odot$ neutron star and its radius R. In the right panel of Fig. 5, we show the correlation between the tidal deformability Λ of a 1.4 $M_\odot$ neutron star and the pressure p_{2n_0} at $n = 2n_0$. We find strong correlations in both cases, the latter suggesting that improved theoretical modeling at $n = 2n_0$ may place stronger constraints on neutron star tidal deformabilities. Our Λ vs R correlation is in very good agreement with that of Ref. [12], which is shown as the dashed curve in the left
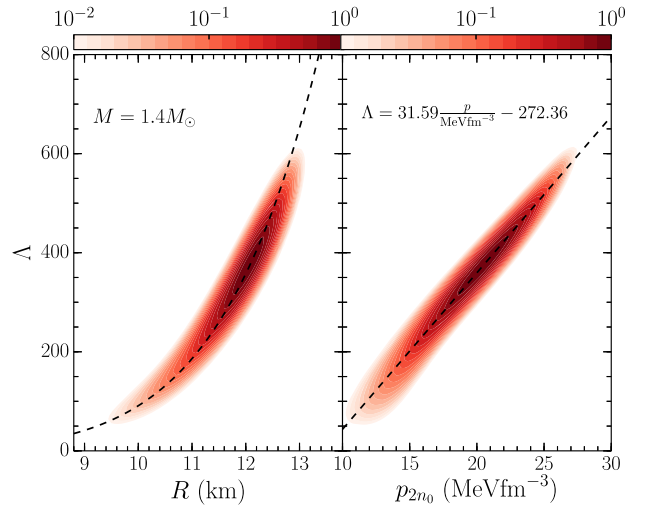

FIG. 5. Probability contour plot for the tidal deformability Λ vs radius R of a 1.4 $M_\odot$ neutron star (left) and Λ vs the pressure p_{2n_0} of neutron star matter at $n = 2n_0$ (right). The dashed line (left) is the empirical relation derived in Ref. [12] and the dashed line (right) is the empirical relation derived in the present analysis.

panel of Fig. 5. In addition, we derive a second empirical relationship, which is approximately linear over the range covered by our results, between the tidal deformability Λ of a 1.4 $M_\odot$ neutron star and the pressure at twice saturation density of the form $\Lambda = 31.59\ (p/\text{MeV fm}^{-3}) - 272.36$. Finally, since neutron star radii are expected to be correlated with the slope of the symmetry energy L at nuclear saturation density, we anticipate a similar correlation between L and the tidal deformability. In Fig. 6, we plot the two-dimensional probability contours for Λ and L for a 1.4 $M_\odot$ neutron star. We naturally expect that larger values of L are correlated with larger values of the tidal deformability since the former gives rise to a stiffer equation of
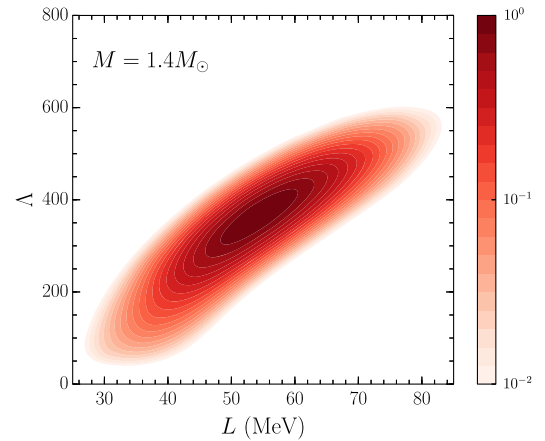

FIG. 6. Probability contour plot for the tidal deformability Λ and isospin-asymmetry energy slope parameter L for a 1.4 $M_\odot$ neutron star.

state and a larger neutron star radius for a given mass. The present modeling, however, suggests that a precise measurement of Λ may not provide a strong constraint on the symmetry energy slope parameter L.

Recently, we became aware of a very similar study [57] that reaches some of the same conclusions as our Letter. The authors of Ref. [57] employ a different set of chiral nuclear potential models to construct the neutron matter equation of state, which they extrapolate to higher densities using piecewise polytropes. In contrast to our equations of state, those in Ref. [57] are strongly constrained by new upper bounds on the maximum neutron star mass. Both analyses, however, point to the importance of lower bounds on the tidal deformability for placing limitations on equation of state modeling. In comparison to Ref. [57], our predictions for the mass vs radius relation are similar but we find radii that are systematically lower by about 0.5 km with a larger uncertainty band of $R_{+2\sigma} - R_{-2\sigma} = 2.51$ km for a $1.4\ M_\odot$ neutron star due to our inclusion of equations of state with $\tilde{\Lambda} < 400$ for equal mass binaries.

In summary, we have computed neutron star masses, radii, and tidal deformabilities from posterior probability distributions obtained from chiral effective field theory priors and likelihood functions derived from empirical data in the vicinity of normal nuclear matter density. We have found that the upper bound on the tidal deformability of a $1.4\ M_\odot$ neutron star inferred from GW170817 is already consistent with the latest theoretical modeling of the equation of state from chiral effective field theory and nuclear experiments, but that lower bounds on Λ appear to be much more important for constraining the equation of state. We have also derived an empirical correlation between the tidal deformability of a $1.4\ M_\odot$ neutron star and the pressure of beta-equilibrated matter at twice nuclear saturation density. Tightening the upper and lower bounds on the tidal deformability with future binary neutron star merger observations, together with upcoming neutron star mass-radius measurements, will be invaluable for further constraining the nuclear equation of state. The present Bayesian modeling provides the framework for such a program.

[*]ylim@tamu.edu

[†]holt@physics.tamu.edu

[1] B. P. Abbott *et al.* (LIGO Scientific Collaboration and Virgo Collaboration), Phys. Rev. Lett. **119**, 161101 (2017).

[2] B. P. Abbott *et al.*, Astrophys. J. Lett. **848**, L12 (2017).

[3] T. Hinderer, Astrophys. J. **677**, 1216 (2008).

[4] J. S. Read, C. Markakis, M. Shibata, K. Uryu, J. D. E. Creighton, and J. L. Friedman, Phys. Rev. D **79**, 124033 (2009).

[5] A. W. Steiner, S. Gandolfi, F. J. Fattoyev, and W. G. Newton, Phys. Rev. C **91**, 015804 (2015).

[6] A. Bauswein, O. Just, H.-T. Janka, and N. Stergioulas, Astrophys. J. Lett. **850**, L34 (2017).

[7] B. Margalit and B. D. Metzger, Astrophys. J. Lett. **850**, L19 (2017).

[8] M. Shibata, S. Fujibayashi, K. Hotokezaka, K. Kiuchi, K. Kyutoku, Y. Sekiguchi, and M. Tanaka, Phys. Rev. D **96**, 123012 (2017).

[9] D. Radice, A. Perego, F. Zappa, and S. Bernuzzi, Astrophys. J. Lett. **852**, L29 (2018).

[10] L. Rezzolla, E. R. Most, and L. R. Weih, Astrophys. J. Lett. **852**, L25 (2018).

[11] M. Ruiz, S. L. Shapiro, and A. Tsokaros, Phys. Rev. D **97**, 021501 (2018).

[12] E. Annala, T. Gorda, A. Kurkela, and A. Vuorinen, Phys. Rev. Lett. **120**, 172703 (2018).

[13] P. G. Krastev and B.-A. Li, arXiv:1801.04620.

[14] S. Postnikov, M. Prakash, and J. M. Lattimer, Phys. Rev. D **82**, 024016 (2010).

[15] T. Hinderer, B. D. Lackey, R. N. Lang, and J. S. Read, Phys. Rev. D **81**, 123016 (2010).

[16] J. S. Read, L. Baiotti, J. D. E. Creighton, J. L. Friedman, B. Giacomazzo, K. Kyutoku, C. Markakis, L. Rezzolla, M. Shibata, and K. Taniguchi, Phys. Rev. D **88**, 044042 (2013).

[17] B. D. Lackey and L. Wade, Phys. Rev. D **91**, 043002 (2015).

[18] K. Hotokezaka, K. Kyutoku, Y.-i. Sekiguchi, and M. Shibata, Phys. Rev. D **93**, 064082 (2016).

[19] C. A. Raithel, F. Özel, and D. Psaltis, Astrophys. J. **857**, L23 (2018).

[20] S. Weinberg, Physica (Amsterdam) **96A**, 327 (1979).

[21] E. Epelbaum, H.-W. Hammer, and U.-G. Meißner, Rev. Mod. Phys. **81**, 1773 (2009).

[22] R. Machleidt and D. R. Entem, Phys. Rep. **503**, 1 (2011).

[23] J. M. Lattimer and M. Prakash, Astrophys. J. **550**, 426 (2001).

[24] C. Y. Tsang, M. B. Tsang, P. Danielewicz, W. G. Lynch, and F. J. Fattoyev, arXiv:1807.06571.

[25] Y. Lim and J. W. Holt, Phys. Rev. C **95**, 065805 (2017).

[26] Z. Zhang, Y. Lim, J. W. Holt, and C.-M. Ko, Phys. Lett. B **777**, 73 (2018).

[27] X. Du, A. W. Steiner, and J. W. Holt, arXiv:1802.09710.

[28] K. Hebeler, J. M. Lattimer, C. J. Pethick, and A. Schwenk, Phys. Rev. Lett. **105**, 161102 (2010).

[29] K. Hebeler, J. M. Lattimer, C. J. Pethick, and A. Schwenk, Astrophys. J. **773**, 11 (2013).

[30] A. Bauswein, H.-T. Janka, K. Hebeler, and A. Schwenk, Phys. Rev. D **86**, 063001 (2012).

[31] R. B. Wiringa, V. Fiks, and A. Fabrocini, Phys. Rev. C **38**, 1010 (1988).

[32] I. Bombaci and U. Lombardo, Phys. Rev. C **44**, 1892 (1991).

[33] C. Wellenhofer, J. W. Holt, and N. Kaiser, Phys. Rev. C **92**, 015801 (2015).

[34] P. Papakonstantinou, T.-S. Park, Y. Lim, and C. H. Hyun, Phys. Rev. C **97**, 014312 (2018).

[35] I. Lagaris and V. Pandharipande, Nucl. Phys. **A369,** 470 (1981).

[36] N. Kaiser, Phys. Rev. C **91,** 065201 (2015).

[37] C. Wellenhofer, J. W. Holt, and N. Kaiser, Phys. Rev. C **93,** 055802 (2016).

[38] J. Margueron, R. Hoffmann Casali, and F. Gulminelli, Phys. Rev. C **97,** 025806 (2018).

[39] J. W. Holt, N. Kaiser, and W. Weise, Prog. Part. Nucl. Phys. **73,** 35 (2013).

[40] J. W. Holt, M. Rho, and W. Weise, Phys. Rept. **621,** 2 (2016).

[41] L. Coraggio, J. W. Holt, N. Itaco, R. Machleidt, and F. Sammarruca, Phys. Rev. C **87,** 014322 (2013).

[42] J. W. Holt and N. Kaiser, Phys. Rev. C **95,** 034326 (2017).

[43] I. Tews, T. Krüger, K. Hebeler, and A. Schwenk, Phys. Rev. Lett. **110,** 032504 (2013).

[44] C. Drischler, A. Carbone, K. Hebeler, and A. Schwenk, Phys. Rev. C **94,** 054307 (2016).

[45] D. R. Entem and R. Machleidt, Phys. Rev. C **68,** 041001 (2003).

[46] L. Coraggio, A. Covello, A. Gargano, N. Itaco, D. R. Entem, T. T. S. Kuo, and R. Machleidt, Phys. Rev. C **75,** 024311 (2007).

[47] L. Coraggio, J. W. Holt, N. Itaco, R. Machleidt, L. E. Marcucci, and F. Sammarruca, Phys. Rev. C **89,** 044321 (2014).

[48] F. Sammarruca, L. Coraggio, J. W. Holt, N. Itaco, R. Machleidt, and L. E. Marcucci, Phys. Rev. C **91,** 054311 (2015).

[49] M. Dutra, O. Lourenco, J. S. Sá Martins, A. Delfino, J. R. Stone, and P. D. Stevenson, Phys. Rev. C **85,** 035201 (2012).

[50] I. Tews, J. M. Lattimer, A. Ohnishi, and E. E. Kolomeitsev, Astrophys. J. **848,** 105 (2017).

[51] J. W. Holt and Y. Lim, Phys. Lett. B **784,** 77 (2018).

[52] A. W. Steiner, J. M. Lattimer, and E. F. Brown, Astrophys. J. **722,** 33 (2010).

[53] H. Krebs, A. Gasparyan, and E. Epelbaum, Phys. Rev. C **85,** 054006 (2012).

[54] M. Hoferichter, J. Ruiz de Elvira, B. Kubis, and Ulf-G. Meißner, Phys. Rev. Lett. **115,** 192301 (2015).

[55] E. Epelbaum, H. Krebs, and U.-G. Meißner, Phys. Rev. Lett. **115,** 122301 (2015).

[56] D. R. Entem, R. Machleidt, and Y. Nosyk, Phys. Rev. C **96,** 024004 (2017).

[57] E. R. Most, L. R. Weih, L. Rezzolla, and J. Schaffner-Bielich, Phys. Rev. Lett. **120,** 261103 (2018).